HHS Public Access

Author manuscript

Nat Immunol. Author manuscript; available in PMC 2019 August 01.

Published in final edited form as:

Nat Immunol. 2018 August ; 19(8): 828–837. doi:10.1038/s41590-018-0155-6.

Translational repression of pre-formed cytokine-encoding mRNA prevents chronic activation of memory T cells

Fiamma Salerno[1], **Sander Engels**[1], **Maartje van den Biggelaar**[2], **Floris P. J. van Alphen**[2], **Aurelie Guislain**[1], **Wanqi Zhao**[1], **Deborah L. Hodge**[3], **Sarah E. Bell**[4], **Jan Paul Medema**[5], **Marieke von Lindern**[1], **Martin Turner**[4], **Howard A. Young**[3], and **Monika C. Wolkers**[1,*]

[1]Sanquin Research, Department of Hematopoiesis, and Landsteiner Laboratory, Academic Medical Centre (AMC), University of Amsterdam, Amsterdam, The Netherlands [2]Sanquin Research, Department of Plasma Proteins, Amsterdam, The Netherlands [3]Laboratory of Experimental Immunology, Cancer and Inflammation Program, Center for Cancer Research, National Cancer Institute at Frederick, MD, USA [4]Laboratory of Lymphocyte Signalling and Development, The Babraham Institute, Babraham, UK [5]Laboratory of Experimental Oncology and Radiobiology (LEXOR), Center for Experimental Molecular Medicine (CEMM), Academic Medical Center (AMC), University of Amsterdam, Amsterdam, The Netherlands

Abstract

Memory T cells are critical for the immune response to recurring infections. Their instantaneous reactivity to pathogens is empowered by the persistent expression of cytokine-encoding mRNAs. How the translation of proteins from pre-formed cytokine-encoding mRNAs is prevented in the absence of infection has remained unclear. Here we found that protein production in memory T cells was blocked via a 3' untranslated region (3'UTR)-mediated process. Germ-line deletion of AU-rich elements (AREs) in the *Ifng*-3'UTR led to chronic cytokine production in memory T cells. This aberrant protein production did not result from increased expression and/or half-life of the mRNA. Instead, AREs blocked the recruitment of cytokine-encoding mRNA to ribosomes, which depended on the ARE-binding protein ZFP36L2. Thus, AREs mediate repression of translation in mouse and human memory T cells by preventing undesirable protein production from pre-formed cytokine-encoding mRNAs in the absence of infection.

[*]**Correspondence to:** Monika Wolkers, Sanquin Research Department of Hematopoiesis, and Landsteiner Laboratory, AMC. Plesmanlaan 125, 1066 CX Amsterdam, The Netherlands. m.wolkers@sanquin.nl. Tel: +31-20-5127003. FAX: +31-20-5123474.

AUTHOR CONTRIBUTIONS

F.S. and M.C.W. designed experiments, F.S., S.E., M.v.B., F.P.J.v.A., A.G., W.Z., S.E.B., and M.C.W. performed experiments and analyzed the data, D.H. and H.A.Y. contributed the ARE-Del mice; S.E.B. and M.T. contributed the CD4cre-ZFP36L2$^{flox/flox}$ mice; M.v.L., M.T., H.A.Y. and J.P.M. provided intellectual input; M.C.W. directed the study; F.S. and M.C.W. wrote the manuscript.

ACCESSION CODES

The materials, data, code and any associated protocols that support the findings of this study are available from the corresponding author upon request. The MS datasets have been deposited in the ProteomeXchange data base under the accession number PXD008051.

COMPETING FINANCIAL INTERESTS STATEMENT

The authors declare no competing financial interests.

Keywords

post-transcriptional regulation; memory T cells; AU-rich elements; Interferon-γ (IFN-γ); cytokines; ZFP36L2/Tis11D; ARE-binding proteins; mRNA translation

Memory T cells (T_M cells) are critical for the immune response against recurring infections. Their longevity and tissue localization allows T_M cells to maintain effective immunity against bacteria, protozoa and viruses[1–3]. A key characteristic of both $CD8^+$ and $CD4^+$ T_M cells is their capacity to produce substantial amounts of effector molecules within a few hours upon re-infection[4–6]. This rapid responsiveness limits pathogen spreading and recruits innate immune cells to the site of infection[7,8]. The swift recall response by T_M cells is supported by changes in chromatin structure and epigenetic modifications that increase transcription rates of genes encoding effector molecules[9–11]. As a result, mRNAs encoding pro-inflammatory cytokines such as interferon gamma (IFN-γ) are increased in human and mouse T_M cells when compared to naive T cells[12–14]. Pre-formed *Ifng* and *Tnf* mRNA is critical for the instantaneous protein production upon T cell activation[15]. Such pre-formed mRNA is advantageous for recall responses, as cytokines can be rapidly produced without initiating transcription. However, chronic cytokine production can elicit severe immunopathology[16,17]. Because pre-formed mRNA is ready to be translated, it is critical that protein production is tightly regulated, and strictly confined to reactivated T_M cells. How chronic and undesired cytokine production from pre-formed mRNA is prevented in T_M cells is to date unknown.

Post-transcriptional regulation is a critical modulator of protein production by regulating mRNA stability, changing mRNA localization and inhibiting protein translation. RNA-binding proteins (RBPs) and non-coding RNAs, such as micro-RNAs, mediate these processes by binding to sequences located in the 3' untranslated region (3'UTR) of the mRNA[18–20]. For instance, global down-regulation of micro-RNAs during T cell activation promotes the acquisition of effector functions[21,22]. Whereas micro-RNAs activity is primarily associated with keeping T cells quiescent, RBPs can directly promote T cell effector responses. The activity of RBPs can be regulated by different post-translational modifications[23,24]. RBPs bind to secondary RNA structures like the constitutive decay element (CDE)[25], or to short single-stranded sequences, such as GU-rich or AU-rich elements (AREs)[26]. The 3'UTR of many cytokines, including *Ifng, Tnf* and *Il2,* contain AREs that consist of one or several AUUUA pentamers[27]. RBP binding to AREs is thought to primarily modulate mRNA stability, which is supported by the observation that many ARE-bearing transcripts display a short mRNA half-life[28].

We show here that rapid mRNA turnover was not sufficient to avoid chronic protein production in T_M cells. Rather, AREs were critical to block translation of pre-formed mRNA, a process that was mediated by the ARE-binding protein ZFP36L2. Thus, T_M cells could contain deployment-ready mRNA for rapid recall responses because the recruitment of pre-formed cytokine mRNA to ribosomes was prevented in the absence of infection.

RESULTS

The 3'UTR of *Ifng* determines protein expression levels in T_M cells

We first examined if the *Ifng* 3'UTR regulated protein production in T_M cells. We fused the murine *Ifng* 3'UTR to a GFP reporter gene (hereafter GFP-*Ifng*3'UTR) under the control of the murine PGK-1 promoter. We retrovirally transduced OTI TCR transgenic $CD8^+$ T cells expressing the congenic marker CD45.1 with GFP-*Ifng*3'UTR, or with GFP that lacked a 3'UTR (hereafter $GFP_{control}$). The next day, 1000 sorted GFP-*Ifng*3'UTR OTI or $GFP_{control}$ OTI cells were transferred into naive C57BL/6J/CD45.2 recipient mice followed by infection with the intracellular bacterium *Listeria monocytogenes* genetically engineered to express ovalbumin (LM-OVA)[29] the next day. We found identical percentages of GFP-*Ifng*3'UTR and of $GFP_{control}$ OTI cells in the blood of recipient mice at all time points measured (Fig. 1a). The $GFP_{control}$ OTI cells expressed constant levels of GFP throughout the infection as determined by the GFP mean fluorescence intensity (GFP-MFI; Supplementary Fig. 1a). In contrast, the GFP-MFI in GFP-*Ifng*3'UTR OT-I cells increased at day 9 post infection, and dropped at day 13, when the infection was resolved (Supplementary Fig. 1a). At day 35 post infection, the GFP-MFI was about six-fold lower for GFP-*Ifng*3'UTR OTI cells than for $GFP_{control}$ OTI cells isolated from blood, liver and spleen (Fig. 1b,c and Supplementary Fig.1b). Reactivation of OTI cells isolated at day 35 post infection with the $OVA_{257–264}$ peptide did not alter the MFI of $GFP_{control}$ OTI cells ($p=0.4$), but increased the expression of GFP-*Ifng*3'UTR compared to non-activated cells ($p=0.01$, Fig. 1b,c).

Spleen-derived $GFP_{control}$ $CD4^+$ and $CD8^+$ T cells from C57BL/6J mice showed high GFP-MFI when cultured in IL-7 for several days in the absence of antigen (hereafter 'resting'), and reactivation for 4h with PMA+ionomycin did not alter the GFP-MFI. In contrast, GFP-*Ifng*3'UTR T cells had low GFP-MFI when resting, and reactivation led to GFP induction (Supplementary Fig. 1c–f). The MFI of endogenous IFN-γ protein was equal in GFP^+ and GFP^- T cells (Supplementary Fig. 1g), indicating that the factors that control protein production were not limiting. Similar results were obtained using the minimal murine *Ifng* promoter[30] (Supplementary Fig. 1h), suggesting that the regulatory capacity of *Ifng* 3'UTR was independent of a specific promoter. Combined, these data implied that the *Ifng* 3'UTR controls protein production in T_M cells.

Conserved AREs in the *Ifng* 3'UTR determine protein expression in T cells

We next defined the regulatory region within the *Ifng* 3'UTR using deletion mutants. Only the reporter constructs containing the first 241 nucleotides of *Ifng* 3'UTR reduced GFP-MFI similar to the GFP-*Ifng*3'UTR reporter in resting OTI cells, and maintained the induction upon 6h reactivation with $OVA_{257–264}$ peptide (Fig. 2a), indicating that this domain was essential to mediate protein expression. The murine *Ifng* 3'UTR contains six class I AREs, of which five are located within the first 241nt (Fig. 2b). Mutating the ARE located outside of the 241nt region of the *Ifng* 3'UTR (GFP-$Ifng_{MUT6}$) did not alter the regulatory capacity of the *Ifng* 3'UTR (Fig. 2c), while the combined site-directed mutation of all five AREs located within the proximal 241nt region (GFP-$Ifng_{MUT1–5}$) completely abrogated its regulatory activity (Fig. 2c). Resting OTI cells transfected with GFP-$Ifng_{MUT1–5}$ had similar

GFP-MFI as $GFP_{control}$, which did not increase upon activation with $OVA_{257–264}$ peptide (Fig. 2c).

Single or double mutants of the five ARE within the proximal 241nt region only marginally altered the GFP-MFI in resting T cells compared to the GFP-*Ifng* 3'UTR, and activation with $OVA_{257–264}$ peptide resulted in an incomplete, but significant increase of GFP-MFI (Supplementary Fig. 2a,b). Mutating the first three AREs (GFP-$Ifng_{MUT1–3}$) clustered at position 74–98nt fully abrogated the induction of GFP-MFI in $OVA_{257–264}$-activated OTI cells, and this deletion only partially blocked protein expression in resting T cells compared to $GFP_{control}$, and GFP-$Ifng_{MUT1–5}$ (Fig. 2d,e). Mutation of the AREs at position 137–141nt and 192–196nt (GFP-$Ifng_{MUT4}$ and GFP-$Ifng_{MUT5}$, respectively) were required to completely block protein production in resting T cells (Fig. 2d).

The ARE-containing region of the *Ifng* 3'UTR is highly conserved in man, mouse and many other mammals (Supplementary Fig. 2c). Human $CD4^+$ and $CD8^+$ T cells transduced with the human GFP-*IFNG* 3'UTR had lower GFP-MFI than the T cells transduced with $GFP_{control}$ (Fig. 2f and Supplementary Fig. 2d). As for mouse $Ifng_{MUT1–3}$ alike, human GFP-$IFNG_{MUT1–3}$ T cells showed higher GFP-MFI than wild-type *GFP-IFNG* 3'UTR T cells, but 4h reactivation with PMA+Ionomycin did not increase GFP-MFI (Fig. 2f and Supplementary Fig. 2d). In contrast, human GFP-$IFNG_{MUT1–5}$ T cells expressed GFP-MFI comparable to $GFP_{control}$ T cells (Fig. 2f and Supplementary Fig. 2c). These findings indicate that the highly conserved proximal region of the *IFNG* 3'UTR in humans and *Ifng* 3'UTR in mice blocks protein production in resting T cells through an ARE-dependent mechanism.

Deletion of *Ifng* 3'UTR AREs causes chronic IFN-γ production in T_M cells

To investigate the effect of deleting AREs from the endogenous *Ifng* encoding mRNA in T_M cells, we crossed OTI mice with mice carring a germline replacement of the ARE-containing region with a random sequence (hereafter IFN-γ-ARE-Del OTI mice)[16]. To compare the expansion kinetics and cytokine production of IFN-γ-ARE-Del OTI cells with wild-type OTI cells in response to LM-OVA infection, we co-transferred equal numbers (500 cells) of sorted naive $CD62L^{hi}CD44^{lo}$IFN-γ-ARE-Del CD45.2 OTI cells and wild-type CD45.1 OTI cells into C57BL/6J CD45.1xCD45.2 recipient mice. This ensured an equivalent bacterial load and a similar cytokine milieu during the course of infection. One day after T cell transfer, recipient mice were infected with LM-OVA. We followed the OTI responses to LM-OVA infection by measuring the percentage of IFN-γ-ARE-Del and wild-type OTI cells of the $CD8^+$ T cell population in the blood. At day 6 and 9 post infection, the percentage of IFN-γ-ARE-Del and wild-type OTI cells was similar. At day 13 when the infection was cleared, OTI cells equally contracted (Fig. 3a). At day 35 post LM-OVA infection, similar percentages of OTI cells were found in blood, spleen, liver and bone marrow of C57BL/6J CD45.1xCD45.2 recipient mice (Fig. 3a and data not shown). In addition, the percentage of $CD44^{hi}CD62L^{lo}CD127^{lo}$ effector T cells (T_{eff}), $CD44^{hi}CD62L^{lo}CD127^{hi}$ effector memory (T_{EM}) and $CD44^{hi}CD62L^{hi}CD127^{hi}$ central memory (T_{CM}) T cells, and the percentage of $KLRG1^{hi}CD127^{lo}$ short-lived effector cells (SLEC) and $KLRG1^{lo}CD127^{hi}$ memory

precurser cells (MPEC) was indistinguishable between IFN-γ-ARE-Del and wild-type OTI cells (Fig. 3b, Supplementary Fig. 3a).

Despite the normal differentiation into T_{EFF} and T_M cells, blood-derived IFN-γ-ARE-Del OTI cells isolated from CD45.1xCD45.2 recipient mice on day 35 post infection produced IFN-γ even in the absence of peptide restimulation, as defined by intracellular cytokine staining after 3h of incubation with brefeldin A (BFA) (Fig. 3c). The IFN-γ production was also detected in spleen, liver and bone marrow-derived IFN-γ-ARE-Del OTI cells 35 days post infection (Fig. 3c), and in spleen and liver-derived IFN-γ-ARE-Del OTI cells 48 days post infection (Supplementary Fig. 3b). In contrast, wild-type OTI cells that were co-transferred into the same CD45.1xCD45.2 recipient mice did not produce IFN-γ (Fig. 3c, Supplementary Fig. 3b). Wild-type and IFN-γ-ARE-Del T cells also did not produce TNF (Fig. 3c). At day 35 post infection all liver and spleen-derived IFN-γ-ARE-Del T cells - T_{EFF}, T_{EM}, T_{CM} cells, SLECs and MPECs- produced IFN-γ, as determined by the percentage and MFI of IFN-γ protein (Fig. 3d; Supplementary Fig. 3c, d).

The expression of *Ifng* mRNA was similar in sorted IFN-γ-ARE-Del and wild-type OTI cells at day 35 post infection (Fig. 3e), indicating that IFN-γ production of IFN-γ-ARE-Del OTI cells did not correlate with increased mRNA expression. To determine whether this leaky IFN-γ production also occurs in other settings, we studied naturally occurring $CD44^{hi}$ memory-like T cells. Similar to infection-induced T_M cells, spleen-derived $CD44^{hi}$ sorted OTI cells mediate protection to LM-OVA infection by rapidly producing IFN-γ upon antigen exposure[31]. $CD44^{hi}$ OTI cells expressed more *Ifng* mRNA than naive $CD44^{lo}$ OTI cells (Supplementary Fig. 3e). Only $CD44^{hi}$ IFN-γ-ARE-Del cells produced IFN-γ *ex vivo* when cultured for 4h in the absence of stimulation (Fig. 3f,g; Supplementary Fig. 3f,g). Yet, the *Ifng* mRNA levels of IFN-γ-ARE-Del OTI cells were comparable to wild-type $CD44^{hi}$ OTI cells (Fig. 3f,g). Again, the IFN-γ production was observed in spleen-derived $CD44^{hi}CD62L^{lo}$ T_{Eff}/T_{EM} cells and in $CD44^{hi}CD62L^{hi}$ T_{CM} cells from IFN-γ-ARE-Del mice (Supplementary Fig. 3f,g), and not from wild-type mice, whereas T cells from both genetic backgrounds expressed identical *Ifng* mRNA levels (Supplementary Fig. 3h). As such, the ARE region within the *Ifng* mRNA controls the production of IFN-γ in Tm cells by post-transcriptional mechanisms.

The ARE-binding protein ZFP36L2 interacts with *Ifng* mRNA

To investigate how AREs prevent the production of IFN-γ in T_M cells, we pulled down the ARE-binding proteins from cytoplasmic cell lysates of *in vitro* expanded, resting primary human T cells using the streptavidin-binding RNA aptamer 4xS1m[32], which expresses the 189nt long ARE region of the human *IFNG*-3'UTR, and analyzed them by mass spectrometry. To reduce false positive results, we included the empty 4xS1m RNA aptamer lackig the ARE region as control (4xS1m-*empty*), and performed the purifications in triplicate. ARE binding was scored positive when a protein was identified in all three samples. This analysis identified 83 proteins that bound *IFNG*-4xS1m but not 4xS1m-*empty*. 57 proteins were significantly enriched (Student *t*-test, false discovery rate [FDR]=0.05, S0=0.4) upon purification with the *IFNG*-4xS1m construct (Fig. 4a). To validate ARE-specific binding, we performed a second purification that included the human

IFNG$_{MUT1–5}$ variant, *IFNG*$_{MUT1–5}$-4xS1m. 80 out of the 83 proteins found in the first purification were also detected in the second purification. Of these, we identified two proteins, ZFP36L1 and ZFP36L2, that interacted with *IFNG*-4xS1m, but not with *IFNG*$_{MUT1–5}$-4xS1m or with 4xS1m-*empty* (Fig. 4a and Supplementary Fig. 4a–d).

ZFP36L1 (TIS11B) and ZFP36L2 (TIS11D) are ZFP36 (tristetraprolin or TTP) family proteins, which bind AREs[33,34]. ZFP36 induces cytokine-encoding mRNA degradation in T cells, and ZFP36-deficient mice develop severe autoimmunity due to excessive cytokine production[35,36]. We detected more *zfp36l2* than *zfp36l1* mRNA in spleen-derived CD44^{hi}CD8^{+} T cells, along with more ZFP36L2 than ZFP36L1 protein (Fig. 4b,c). Furthermore, ZFP36L2 protein expression was comparable in naïve T cells, in CD44^{hi} T_M cells and in PMA+Ionomycin reactivated T_M cells, while ZFP36L1 was only detectable upon T cell activation (Supplementary Fig. 4e). Native RNA immunoprecipitation (i.e. without cross-linking) showed that *Ifng* mRNA was enriched in ZFP36L2 pull-downs from resting T cells, but not from resting IFN-γ-ARE-Del T cells (Fig. 4d). As such, ZFP36L2 interacts specifically with the ARE region of the *Ifng* 3'UTR.

ZFP36L2 represses IFN-γ production independently of mRNA stability

Next, we used mice with a conditional deletion of ZFP36L2 in the T cell lineage[37] to assess the role of ZFP36L2 deficiency in CD44^{hi} memory-like T cells. CD4-Cre Zfp36l2$^{fl/fl}$ mice (hereafter Zfp36l2^{cKO}) had a similar percentage of CD8^{+} and CD4^{+} T_{EFF}, T_{EM} and T_{CM} cell subsets in the spleen as the wild-type littermates (Supplementary Fig. 5a). However, spleen-derived CD44^{hi} CD8^{+} and CD4^{+} T cells from Zfp36l2^{cKO} mice, but not from wild-type littermates, produced IFN-γ in the absence of stimulation (Fig. 5a,b), whereas *Ifng* mRNA amounts were comparable to wild-type CD44^{hi} T cells (Fig. 5a,b).

We next tested if loss of ZFP36L2 also affected the GFP reporter constructs. We transduced wild-type and Zfp36l2^{cKO} T cells with GFP$_{control}$, GFP-*Ifng*3'UTR or GFP-*Ifng*$_{MUT1–5}$. The GFP-MFI of GFP-*Ifng*$_{MUT1–5}$ T cells and GFP$_{control}$ T cells was comparable in resting wild-type and Zfp36l2^{cKO} T cells (Fig. 5c,d). In contrast, GFP-MFI was substantially increased in GFP-*Ifng* 3'UTR CD8^{+} and in CD4^{+} Zfp36l2^{cKO} T cells compared to wild-type T cells (Fig. 5c,d), indicating that ZFP36L2 repressed IFN-γ production in T cells.

AREs are primarily associated with the regulation of mRNA stability[16,17,35,38]. The overall amount of mRNA depends on the transcription rate and the rate of mRNA decay. We measured the rate of mRNA decay by treating resting OTI cells with the polymerase II transcription inhibitor actinomycin D (ActD). *Ifng* mRNA had a longer half-life in IFN-γ-ARE-Del OTI cells ($t_{1/2}$ >120min) than in wild-type OTI cells ($t_{1/2}$ ~30min; Fig. 5e). The half-life of *Ifng* dropped to $t_{1/2}$ ~60min in sorted CD44^{hi} IFN-γ-ARE-Del OTI cells, compared to $t_{1/2}$ ~30min in wild-type OTI cells (Fig. 5f). Following 120 min of ActD treatment the decay of *Ifng* mRNA in IFN-γ-ARE-Del OTI cells was similar to that of wild-type OTI cells (Fig. 5f), indicating that the *Ifng* mRNA stability *ex vivo* is substantially lower than *in vitro*. This was not the case for other transcripts, because *Tnf* remained unstable, and *18S* remained stable (Supplementary Fig. 5b–e). Similar data were obtained using polyclonal CD4^{+} and CD8^{+}CD44^{hi} T cells from IFN-γ-ARE-DEL mice (Fig. 5g; Supplementary Fig. 5f). The rate of *Ifng* mRNA decay in Zfp36l2^{cKO} CD4^{+} and CD8^{+}

CD44^{hi} T cells was comparable to that of IFN-γ-ARE-DEL T cells (Fig. 5h; Supplementary Fig. 5g), indicating the ARE-independent degradation of *Ifng* mRNA did not require ZFP36L2. In addition, the amount of miR-29a/b, which can affect *Ifng* mRNA expression[39,40], and the expression of *Tbx21* and *Eomesodermin* mRNA, which encode the transcription factors T-bet and Eomes, were similar in IFN-γ-ARE-Del and wild-type CD44^{hi} T_M cells (Supplementary Fig. 5h), suggesting that the expression of these factors was not influenced by IFN-γ-ARE-Del-mediated alterations in T_M cells. As such, *Ifng*-AREs determine the *Ifng* mRNA stability depending on the activation status of T cells, and they do so in a ZFP36L2-independent manner.

ZFP36L2 blocks the association of *Ifng* mRNA to ribosomes in T_M cells

We next examined if AREs modulated transcription and translation of *Ifng* mRNA in T_M cells. We treated spleen-derived IFN-γ-ARE-Del CD44^{hi} memory-like T cells with ActD, or the translation inhibitor cycloheximide (CHX) and measured the IFN-γ production in the absence of stimulation. Blocking transcription with ActD did not interfere with IFN-γ production in IFN-γ-ARE-Del CD44^{hi} T cells (Fig. 6a,b). We did not detect TNF production in these cells, and cell viability or the surface markers CD8 and CD44 were unaltered (Supplementary Fig. 6a). In contrast, treatment with CHX, which inhibits protein translation, blocked the production of IFN-γ in IFN-γ-ARE-Del CD44^{hi} T cells compared to ActD-treated cells (Fig. 6a,b), indicating that the IFN-γ production depended on translation and that the pre-formed *Ifng* mRNA serves as template for protein production in IFN-γ-ARE-Del CD44^{hi} T_M cells.

To test whether AREs impaired the translation of pre-formed *Ifng* mRNA, we measured the association of *Ifng* mRNA with the ribosomes in spleen-derived IFN-γ-ARE-Del or wild-type CD44^{hi} T cells. The heavy fraction of cytosolic extracts was pelleted by sucrose cushion centrifugation to enrich for ribosomes[41]. As control, half of the each cytosolic extract was treated with 20mM EDTA, which dissociates ribosomal and ribosome-associated proteins from mRNA[41] (Supplementary Fig. 6b). mRNA levels measured from this control sample included residual binding of *Ifng* mRNA to ribosomes and unbound *Ifng* mRNA, and was substracted from the pellets of EDTA-untreated sucrose cushions. Only the *Ifng* mRNA from IFN-γ-ARE-Del CD44^{hi} T cells, but not from wild-type CD44^{hi} T cells associated with ribosomes (Fig. 6c). The association of control mRNAs *Tnf* and *18S* was comparable between wild-type and IFN-γ-ARE-Del CD44^{hi} T cells (Supplementary Fig. 6c,d). Notably, also the *Ifng* mRNA from CD44^{hi}CD4^{+} and CD44^{hi}CD8^{+} Zfp36l2^{cKO} T cells associated with ribosomes (Fig. 6d,e), indicating that the recruitment of *Ifng* mRNA to the ribosome depended at least in part on ZFP36L2. Thus, AREs within the *Ifng* mRNA and ZFP36L2 suppress the translation of IFN-γ protein from pre-existing mRNA in T_M cells.

ZFP36L2 binds to pre-formed mRNA in memory T cells

To determine if ZFP36L2 blocked the translation of other ARE-containing mRNAs that are rapidly translated in T_M cells upon activation, we sorted spleen-derived CD44^{hi} memory-like OTI cells and performed mass spectrometry on untreated cells, and on T cells activated for 2h with $OVA_{257–264}$ peptide. Of the 5490 identified proteins, 54 significantly altered their expression profile upon T cell activation (Student *t*-test, FDR=0.05, S0=0.4; Fig. 7a,

Supplementary Fig. 7a). 17 proteins were significantly less abundant in stimulated T cells, including CD62L (Sell, Fig. 7a), which is rapidly downregulated upon T cell activation. Conversely, 37 proteins were significantly induced in stimulated CD44^{hi} OTI cells, including the early activation marker CD69 and the pro-inflammatory cytokines IFN-γ, TNF and IL-2 (Fig. 7a). Of note, 32 of these 37 proteins were generated from ARE-containing mRNAs (Fig. 7a; Supplementary Fig. 7a).

We next determined the mRNA levels of these rapidly induced proteins in T_M cells. 52 out of the 54 proteins that altered their expression profile upon activation of CD44^{hi} OTI cells were annotated in T_{EM} and T_{CM} cells specific for the lymphochoriomeningitis virus (LCMV)[42]. The mRNAs for the 17 proteins that were enriched in the CD44^{hi} OTI cells were also expressed in LCMV-specific T_{EM} and T_{CM} cells (Fig. 7b, Supplementary Fig. 7b). The mRNAs of the 35 proteins that were rapidly induced in CD44^{hi} OTI cells greatly varied in expression in T_{EM} and T_{CM} cells (Fig. 7b, Supplementary Fig. 7b). LCMV-specific T_{EM} and T_{CM} cells expressed the mRNA for 29 of the 35 (82.9%) rapidly generated proteins (Fig. 7b, Supplementary Fig. 7b). For 22 of these 35 proteins (62.9%), the peptide abundance was below detection limit in non-activated CD44^{hi} T cells (Supplementary Fig. 7a), indicating that these 22 mRNAs are putatively blocked from translation in T_M cells.

ZFP36L2 binds to ARE-containing mRNA with a tandem zinc finger[43] that requires two AREs for interaction. Of the 35 rapidly-induced proteins, 26 ARE-containing transcripts encompassed at least 2 AREs (defined as AUUUA) within the 3'UTR (Supplementary Table 1). We focused on 11 putative target genes that fulfilled the following criteria: they contained 2 AREs in most of their transcript variants (Supplementary Table 1), and they expressed pre-formed mRNA in T_M cells (Supplementary Fig. 7b). We measured ZFP36L2 binding to these endogenously expressed mRNAs using native RNA-immunoprecipitation in resting OTI cells. Of the 11 tested mRNAs, 6 mRNAs were significantly enriched in resting T cells compared to the IgG control pull down: *Ifng, Tnf, Irf4, Junb, Zfp36l1* and *Pim1* (Fig. 7c), indicating that ZFP36L2 targets several ARE-containing pre-formed mRNAs T_M cells .

ZFP36L2 rapidly releases pre-formed mRNA upon activation

Because pre-formed mRNA drives rapid cytokine production upon T cell activation[15], we tested if T cell activation supports the release of pre-formed mRNA from ZFP36L2. As determined by RNA-immunoprecipitation, ZFP36L2 binding to *Ifng* mRNA was significantly reduced in OTI cells reactivated with $OVA_{257–264}$ for 2h compared to non-activated resting OTI cells (Fig. 7d). Of note, loss of mRNA binding upon reactivation coincided with rapid downregulation of *Zfp36l2* mRNA, but ZFP36L2 protein remained unaltered (Supplementary Fig. 7d). ZFP36L2 also rapidly dissociated from *Tnf* and *Pim1* mRNA upon T cell activation, while its binding to *Irf4, Junb* and *Zfp36l1* mRNA did not change compared to non-activated T cells (Fig. 7d). Peptides for IFN-γ, TNF and Pim1 were below detection limit in non-activated CD44^{hi} T cells in the proteomics analysis (Supplementary Fig. 7a), further pointing to a block of mRNA translation. *Tnf* mRNA was significantly enriched in the ribosome-enriched fraction of Zfp36l2^{cKO} CD8$^+$ and CD4$^+$ CD44^{hi} T cells compared to wild-type T cells (Fig. 7e), and TNF production was found in CD8$^+$ and CD4$^+$ CD44^{hi} T cells in the absence of stimulation (Fig. 7f). These observations

thus show that ZFP36L2 suppresses the translation of several target mRNAs in memory T cells.

DISCUSSION

Here, we show that the translation of pre-formed *Ifng* mRNA was actively repressed in T_M cells. All five highly conserved AREs of the *Ifng* 3'UTR contributed to the translational block, which may render this regulatory mechanism refractory to single nucleotide polymorphisms. The ARE-binding protein ZFP36L2 mediated the translational silencing of pre-formed mRNA in T_M cells. Germline deletion of the entire ARE-containing region and ZFP36L2 deficiency in T_M cells caused aberrant recruitment of pre-formed *Ifng* mRNA to ribosomes, and led to IFN-γ protein production in the absence of activation. ZFP36L2 not only controlled the translation of *Ifng,* but also of *Tnf* and *Pim1* mRNA encoding for other rapidly induced proteins. Thus, the ARE-dependent inhibition of translation keeps T_M cells silent in the absence of infection.

T_M cells continuously receive tonic signals through cytokines and/or through their TCR that support their maintenance[44–46]. Tonic signaling drives the constitutive expression of unstable cytokine mRNA[47]. We postulate that the active suppression of cytokine production is required to maintain T_M cells silent in the absence of the infection. Whether tonic signaling also controls the function of ZFP36L2 is yet to be determined. Once T_M cells become reactivated, pre-formed mRNA is rapidly disengaged by ZFP36L2, allowing for the immediate production of protein. Because the expression of ZFP36L2 protein was not altered, ZFP36L2 could be ready for rapid re-engagement, target other mRNAs, or exert different functions in stimulated T cells.

ZFP36L1 mRNA and protein expression was lower in T_M cells than that of ZFP36L2, and the contribution of ZFP36L1 to block translation in T_M cells may therefore be limited. However, because ZFP36L2-binding to mRNA is rapidly lost upon activation, ARE-mediated regulation may be highly versatile and dependent on the context. It is conceivable that ZFP36 and ZFP36L1 drive post-transcriptional events at other stages of T cell differentation or activation. This also may hold true for other RBPs such as TIA, which limits excessive TNF production through a translational block in LPS-stimulated macrophages[48]. Similar regulatory mechanisms may also occur in T cells, depending on the activation status.

The biological relevance of ARE-mediated cytokine production was highlighted by the germline deletion of AREs in the *Ifng* 3'UTR or the *Tnf* 3'UTR that lead to chronic cytokine production and consequentially to autoimmune disease in mice[16,17]. 16% of human protein-coding genes are thought to contain AREs[49]. Cytokine and chemokine mRNA transcripts are highly enriched for these sequences[20,26], pointing to a specific role of AREs in the effector function of T cells. Also the rapidly responding NK cells, NKT cells and in myeloid cells constitutively express mRNA encoding for effector molecules[50,51]. Conversely, self-reactive $CD4^+$ T cells maintain their anergic phenotype by blocking the translation of cytokine mRNAs[52]. It is therefore tempting to speculate that the ARE-

dependent translational repression described here is more broadly employed to regulate immune responses.

In conclusion, we identified a conserved mechanism that tightly regulates the translation of pre-formed cytokine mRNAs in $CD8^+$ and $CD4^+$ T_M cells. Considering that tissue-resident $CD8^+$ T_M cells express even higher levels of mRNA encoding for effector molecules than circulating T_M cells[53], our findings suggest that manipulation of ARE-mediated post-transcriptional control may be exploited to rectify impaired T cell responses in tissues, as for example against tumors.

ONLINE METHODS

Mice and cell culture

Mice were obtained from Charles River, or housed and bred in-house at the Netherlands Cancer Institute (NCI). IFN-γ ARE-Del mice were generated as previously described[16] and crossed to C57BL/6J.OTI T cell receptor (TCR) transgenic mice (OTI). Mice carrying a conditional allele of *Zfp36l2* have been previously described[37] and were crossed to mice in which the Cre recombinase is expressed under the control of mouse CD4 regulatory elements (TG(CD4-cre)1Cwi) to obtain deletion specifically in T cells[55]. Experiments were performed in accordance with institutional and national guidelines and approved by the Experimental Animal Committee at the NCI.

Cells were cultured at 37°C and 5% CO_2 in IMDM (GIBCO-BRL) containing 8% FCS, 2mM L-glutamine and Pen/Strep, and for mouse cells supplemented with 15μM 2-mercaptoethanol.

Cloning

Gene-specific 3'UTRs were amplified from genomic DNA of a C57BL/6J mouse, or from human genomic DNA (sequences upon request). The 3'UTR variants were cloned into the ClaI site of pRETRO-SUPER GFP[56] downstream of GFP. 189nt of the human *IFNG* 3'UTR were cloned into the pSP73–4xS1m[32]. The region containing the streptavidin binding sites was reversed using the two BglII sites, and the *IFNG* 3'UTR was inserted to the 5' end of the S1m motifs. Prior to *in vitro* transcription, the pSP73–4xS1m construct was linearized with NdeI. ARE-mutants with a substitution of AUUUA sequence with AAAAA were obtained from GeneScript, and subcloned into pRS-GFP or pSP73–4xS1m. Sequences were confirmed by sequence analysis.

T cell activation and retroviral transduction

1.5×10^6 human PBMCs were activated in a 24-well plate for 40h with plate-bound anti-CD3/CD28 (1μg/ml each, eBioscience). Retroviral transduction was performed with Retronectin (Takara) as described[57], and cells were maintained in culture in the presence of 20ng/ml recombinant human Interleukin 7 (PeproTech).

1×10^6 CD8-purified OTI T cells (Miltenyi CD8 isolation kit; 90–99% purity) were co-cultured for 20h with 0.1×10^6 pre-seeded MEC.B7.SigOVA cells as described[58]. 3×10^6 C57BL/6J splenocytes were activated for 48h with Concanavalin A (2μg/ml, Sigma) and

recombinant murine Interleukin 7 (rmIL-7, 1ng/ml, PeproTech), or with plate-bound anti-CD3 (2μg/ml, eBioscience) and soluble anti-CD28 (1μg/ml, Bioceros) antibodies. Cells were harvested and retrovirally transduced as described[59]. T cells were maintained with 10ng/ml rmIL-7 and reactivated with 100nM or 1μM $OVA_{257–264}$, or with 10ng/ml PMA/1μM ionomycin (Sigma).

FACS-sorted $CD8^+$ and $CD4^+$ $CD44^{hi}$ T cells were isolated from spleen or liver of 6–9 week-old mice. T cells were incubated for 4h with brefeldin A (BFA), with or without 1μg/ml Actinomycin D (ActD) or 10μg/ml cycloheximide (CHX) (Sigma).

Adoptive T cell transfer and *Listeria monocytogenes*-OVA infection

GFP-expressing OTI T cells were purified with Lympholyte M (Cedarlane) and FACS-sorted for GFP expression. Naive $CD8^+CD44^{lo}CD62L^{hi}$ WT and IFN-γ-ARE-Del OTI T cells were FACS-sorted from splenocytes. 1000 GFP^+ OTI T cells, or 500 naive WT OTI/ $CD45.1^+$ together with 500 naive IFN-γ-ARE-Del OTI/ $CD45.2^+$ T cells were adoptively transferred into recipient mice. The next day, mice were infected *i.v.* with 2.5×10^3 or 2.5×10^4 of *L. monocytogenes* strain expressing Ovalbumin (LM-OVA). Peripheral blood was drawn to monitor T cell responses. 35–48 days after infection, spleen, liver and bone marrow cells were incubated with brefeldin A alone, or reactivated for 6h with 1μg/ml $OVA_{257–264}$, and intracellular staining for IFN-γ was performed.

Flow cytometry

Mouse T cells were labeled for 20min at 4°C with anti-CD3 (17A2), anti-CD4 (GK1.5), anti-CD8 (53–6.7), anti-CD45.1 (A20), anti-CD45.2 (104), anti-$V\beta_{5.1–5.2}$ (MR9–4), anti-CD44 (IM7), anti-CD62L (MEL-14), anti-CD127 (A7R34), KLRG1 (MAFA), anti-IFN-γ (XMG1.2) and anti-TNF-α (MP6-XT22) (all eBioscience). Human T cells were labeled with anti-CD3 (UCHT1, Beckman Coulter), anti-CD4 (SK3, BD Biosciences), anti-CD8 (SK1, BD Biosciences). Dead cells were excluded with 1ng/ml TO-PRO-3 iodide (Sigma-Aldrich), or Near-IR (L10119, Life Technology). Intracellular cytokine staining was performed with the cytofix/cytoperm kit (BD Biosciences). Flow cytometry analysis was performed on LSR-II and LSR Fortessa (BD Biosciences). Data were analyzed with FlowJo software (Tree Star, version 7.6.5 and version 10). Representative flow cytometry gating strategies are found in Fig S9.

Quantitative PCR analysis

Total RNA was extracted using Trizol (Invitrogen) and cDNA was synthesized with SuperScript III (Invitrogen), unless differently specified. MiR were extracted from FACS-sorted $CD8^+CD44^{hi}$ WT and IFN-γ-ARE-Del OTI T cells using Total RNA Purification Plus Kit (Norgen Biotek), and cDNA was synthesized with miScript II RT kit (Qiagen). RT-PCR was performed with triplicate reactions using SYBR green on a StepOne Plus (both Applied Biosystems) (primer sequences see[58]). C_t values were normalized to L32 levels and confirmed with 18S.

RNA immunoprecipitation and Western Blot

Cytoplasmic lysates of resting WT or IFN-γ-ARE-Del OTI T cells (250×10^6 cells per condition) were prepared using lysis buffer (10mM HEPES pH 7.0, 100mM KCl, 5mM $MgCl_2$, 0.5% NP40) freshly supplemented with 1mM DTT, 40U/ml RNase OUT (both Invitrogen), 0.4mM vanadylribonucleoside complex RNase inhibitor (NEB) and 1% EDTA-free protease/phosphatase inhibitor cocktail (Thermo Scientific). Protein G dynabeads (Thermo Scientific) were prepared as previously described[60]. The lysate was immunoprecipitated for 2h at 4°C with a rabbit anti-ZFP36L2 polyclonal antibody (ab70775) or a rabbit polyclonal IgG isotype control (ab27478, both Abcam). RNA was extracted directly from beads by using Trizol, and mRNA expression was measured by RT-PCR as described above. Specificity of the RNA-IP assay was tested by western blot using a rat pan-ZFP36 antibody generated in the laboratory of M. Turner (unpublished data). This antibody is directed against the C terminus of ZFP36L1 and recognizes all three ZFP36 family members.

1×10^6 FACS-sorted $CD8^+CD44^{low}$ and $CD8CD44^{hi}$ T cells were lysed according to standard procedures. Proteins were separated on a 10% SDS-PAGE gel and transferred onto a nitrocellulose membrane by iBlot (Thermo). Rabbit anti-ZFP36L1 polyclonal antibody (ab42473), rabbit anti-ZFP36L2 polyclonal antibody (ab70775, both Abcam), mouse anti-RhoGDI monoclonal antibody (MAB9959, Abnova), mouse anti-GAPDH monoclonal antibody (MAB374, Millipore), and a rat pan-ZFP36 antibody were used as primary antibodies, followed by goat anti-rabbit-HRP (4050–05), goat anti-mouse-HRP (1031–05, both Southern Biotech), or goat anti-rat-HRP (31470, Invitrogen) secondary antibodies.

Sucrose cushion

1×10^6 FACS-sorted $CD8^+$ $CD44^{hi}$ WT or IFN-γ-ARE-Del OTI T cells were lysed in modified polysome buffer (20mM Tris-HCl pH 7.5, 300 mM KCl, 5mM $MgCl_2$, 0.50% NP40) freshly supplemented with 2mM DTT, 40U/ml RNase OUT, and 10μg/ml CHX. Total cell lysate was treated or not with 20mM EDTA pH 8.0 (Invitrogen), layered over a 20% sucrose cushion and then centrifuged at 37,500 rpm at 4°C for 2 hours in a SW60Ti swing out rotor ultracentrifuge (Beckman coulter). RNA was isolated from the pellet using Total RNA Purification Plus Kit (Norgen Biotek), and mRNA expression levels were analyzed by RT-PCR. The distribution of transcripts within the ribosome-enriched fraction was calculated as fold increase relative to the amount of transcript precipitated in the corresponding EDTA treated sample.

4xS1m RNA aptamer-protein pull down

Human resting T cells were washed with PBS and the cell pellet was snap frozen in liquid nitrogen. The cell pellet was homogenized using 5mm steel beads and a tissue lyser (Qiagen TissueLyser II) at 25 Hz for 15 sec per 6 times. The homogenate was then solubilized and pre-cleared as previously described[32]. The 4xS1m RNA aptamers containing or not the 189 nt of the human *IFNG* 3'UTR were *in vitro* transcribed using ampliscribe T7-flash transcription kit (Epicentre) and coupled to Streptavidin Sepharose High Performance beads (GE Healthcare) as described[32]. RNA-coupled beads and cell lysate were incubated for 3.5h at 4°C under rotation in the presence of 60U RNasin (Ambion). For each pull-down, about

30μg *in vitro* transcribed RNA and 10mg protein were used. RNA-bound proteins were eluted by adding 1μg RNaseA (Thermo Scientific) and 100μl 100mM Tris-Hcl pH 7.5 (Gibco-Invitrogen). Proteins were reduced, alkylated and digested into peptides using trypsin. Peptides were desalted and concentrated using Empore-C18 StageTips[61] and eluted with 0.5% (v/v) acetic acid, 80 % (v/v) acetonitrile. Sample volume was reduced by SpeedVac and supplemented with 2% acetonitrile, 0.1% TFA.

Proteomic analysis of OTI memory T cells

Triplicates of 2×10^6 FACS-sorted $CD8^+$ $CD44^{hi}$ OTI T cells were incubated for 2h in IMDM containing 5% FCS and 1μg/ml BrfA with or without the presence of 100nM $OVA_{257–264}$ peptide. Cells were washed twice with ice-cold PBS and cell pellets were snap frozen in liquid nitrogen. Cells were lysed in 40μl 1% Sodium Deoxy Cholate, 40mM Chloro Acetamide (both Sigma Aldrich), 10mM TCEP (Thermo Scientific), and 100mM Tris-Hcl pH 8 (Life Technologies), boiled at 95° for 5 minutes and sonicated for 10 minutes in a Sonifier bath (Branson). An equal volume of 50mM ammonium bicarbonate (Sigma Aldrich) was added, containing 600ng Trypsin Gold (Promega). Samples were digested overnight at room temperature, acidified by addition of 1μl trifluoroacetic acid (Thermo Scientific) and loaded on in-house prepared SDB-RPS StageTips (Empore). Peptides were desalted and eluted in three fractions by increasing concentrations of ammonium formate (100mM and 150mM) or 5% (v/v) ammonium hydroxide and acetonitrile (40%, 60% and 80% v/v)[62]. Sample volume was reduced by SpeedVac and supplemented with 2% acetonitrile, 0.1% TFA.

Mass spectrometry data acquisition

Tryptic peptides were separated by nanoscale C18 reverse chromatography coupled on line to an Orbitrap Fusion Tribrid mass spectrometer via a NanoElectroSpray Ion Source (both Thermo Scientific). Peptides were loaded on a 20 cm 75–360μm inner-outer diameter fused silica emitter (New Objective) packed in-house with ReproSil-Pur C18-AQ, 1.9μm resin (Dr Maisch GmbH). The column was installed on a Dionex Ultimate3000 RSLC nanoSystem (Thermo Scientific) using a MicroTee union formatted for 360μm outer diameter columns (IDEX) and a liquid junction. The spray voltage was set to 2.15 kV. Buffer A was composed of 0.5% acetic acid and buffer B of 0.5% acetic acid, 80% acetonitrile. Peptides were loaded for 17 min at 300nl/min at 5% buffer B, equilibrated for 5 minutes at 5% buffer B (17–22min) and eluted by increasing buffer B from 5–15% (22–87min) and 15–38% (87–147min), followed by a 10 minute wash to 90% and a 5min regeneration to 5%. Survey scans of peptide precursors from 400 to 1500 m/z were performed at 120K resolution (at 200 m/z) with a 1.5×10^5 ion count target. Tandem mass spectrometry was performed by isolation with the quadrupole with isolation window 1.6, HCD fragmentation with normalized collision energy of 30, and rapid scan mass spectrometry analysis in the ion trap. The MS2 ion count target was set to 104 and the max injection time was 35ms. Only those precursors with charge state 2–7 were sampled for MS2. The dynamic exclusion duration was set to 60s with a 10ppm tolerance around the selected precursor and its isotopes. Monoisotopic precursor selection was turned on. The instrument was run in top speed mode with 3s cycles. All data were acquired with Xcalibur software.

Mass spectrometry data analysis

The RAW mass spectrometry files were processed with the MaxQuant computational platform, 1.5.0.25 (RNA pull down) or 1.6.0.13 (memory OTI T cells)[63]. Proteins and peptides were identified using the Andromeda search engine by querying the human Uniprot database (downloaded February 2015, 89796 entries) for the RNA pull down, or the mouse Uniprot database (downloaded August 18, 2017, 51434 entries) for analysis of memory OTI T cells. Standard settings with the additional options match between runs, Label Free Quantification (LFQ), and unique peptides for quantification were selected. The generated 'proteingroups.txt' table was filtered for potential contaminants and reverse hits using Perseus 1.5.0.31 (RNA pull down) or 1.5.1.6 (memory OTI T cells). The LFQ values were transformed in log2 scale, the triplicates per experimental condition grouped, and proteins were filtered for at least three valid values in one of the experimental groups. Missing values were imputed by normal distribution (width=0.3, shift=1.8), assuming these proteins were close to the detection limit. To identify the proteins with the most prominent differences, we performed a two-sided *t*-test using an FDR of 5% and S0 of 0.4 (Volcano plot). Mass spectrometry data of resting and activated memory T cells (Fig. 7 and Supplementary Fig. 7) are deposited at PRIDE: PXD008051.

mRNA expression analysis and ARE determination

mRNA expression of LCMV-specific spleen-derived central memory (CM) and effector memory (EM) T cells was extracted from Mackay *et al.*[42] (GEO accession number: GSE70813). Reads per million mapped reads (RPM) were transformed as log2-normalized counts using DESeq2[64].

To determine the presence of ARE sequences in mRNAs, the 3'UTR sequences of all murine transcripts were downloaded from Ensembl BioMart (release May 2015) and compared to transcripts present in the RNAseq data set of memory T cells[42]. AREs (sequence motif ATTTA) were counted in all 3'UTR variants. When multiple transcripts were present for a gene, we used the minimum, maximum, and average count of AREs. Resulting data were combined with gene expession data by gene symbols.

Statistical analysis

Statistical analysis between groups was performed with GraphPad Prism 6, using the 2-tailed Student *t* test when comparing 2 groups, or one-way ANOVA test with Dunnett correction when comparing > 2 groups. *P* values <0.05 were considered statistically significant.

Supplementary Material

Refer to Web version on PubMed Central for supplementary material.

ACKNOWLEDGEMENTS

We thank the animal caretakers of the NKI and the FACS-sorting facility of Sanquin Research and the Babraham Institute for excellent assistance. We thank D. Zehn for the LM-OVA strain, J. Rohr for listeria cultures, H. Meijer for sharing the sucrose cushion protocol, G. Stoecklin for the 4xS1m aptamer construct, R. Arens, T. Schumacher and J. den Haan for providing mice, S. Libregts, B. van Steensel, K. Moore and B. Nicolet for technical help and

advice, and D. Amsen, M. Nolte, and R. van Lier for critical reading of the manuscript. M.T. and S.E.B. are supported by the Biotechnology and Biological Sciences Research Council. D.H. and H.A.Y. are funded through the intramural research program of the U.S. NCI/NIH. The use of materials and reagents does not imply any endorsement of these products by the U.S. government. This research was supported by the Dutch Science Foundation (VENI grant 916.76.127/VIDI grant 917.14.314, to M.C.W.).

REFERENCES

1. Masopust D & Schenkel JM The integration of T cell migration, differentiation and function. Nature reviews 13, 309–320 (2013).
2. Sheridan BS & Lefrancois L Regional and mucosal memory T cells. Nat Immunol 12, 485–491 (2011). [PubMed: 21739671]
3. Harty JT, Tvinnereim AR & White DW CD8+ T cell effector mechanisms in resistance to infection. Annu Rev Immunol 18, 275–308 (2000). [PubMed: 10837060]
4. Veiga-Fernandes H, Walter U, Bourgeois C, McLean A & Rocha B Response of naive and memory CD8+ T cells to antigen stimulation in vivo. Nat Immunol 1, 47–53 (2000). [PubMed: 10881174]
5. London CA, Lodge MP & Abbas AK Functional responses and costimulator dependence of memory CD4+ T cells. J Immunol 164, 265–272 (2000). [PubMed: 10605020]
6. Whitmire JK, Eam B & Whitton JL Tentative T cells: memory cells are quick to respond, but slow to divide. PLoS Pathog 4, e1000041 (2008).
7. Guidotti LG & Chisari FV Noncytolytic control of viral infections by the innate and adaptive immune response. Annu Rev Immunol 19, 65–91 (2001). [PubMed: 11244031]
8. Soudja SM, Ruiz AL, Marie JC & Lauvau G Inflammatory monocytes activate memory CD8(+) T and innate NK lymphocytes independent of cognate antigen during microbial pathogen invasion. Immunity 37, 549–562 (2012). [PubMed: 22940097]
9. Weng NP, Araki Y & Subedi K The molecular basis of the memory T cell response: differential gene expression and its epigenetic regulation. Nature reviews 12, 306–315 (2012).
10. Wherry EJ et al. Molecular signature of CD8+ T cell exhaustion during chronic viral infection. Immunity 27, 670–684 (2007). [PubMed: 17950003]
11. Philip M et al. Chromatin states define tumour-specific T cell dysfunction and reprogramming. Nature 545, 452–456 (2017). [PubMed: 28514453]
12. Kaech SM, Hemby S, Kersh E & Ahmed R Molecular and functional profiling of memory CD8 T cell differentiation. Cell 111, 837–851 (2002). [PubMed: 12526810]
13. Swanson BJ, Murakami M, Mitchell TC, Kappler J & Marrack P RANTES production by memory phenotype T cells is controlled by a posttranscriptional, TCR-dependent process. Immunity 17, 605–615 (2002). [PubMed: 12433367]
14. Willinger T, Freeman T, Hasegawa H, McMichael AJ & Callan MF Molecular signatures distinguish human central memory from effector memory CD8 T cell subsets. J Immunol 175, 5895–5903 (2005). [PubMed: 16237082]
15. Salerno F, Paolini NA, Stark R, von Lindern M & Wolkers MC Distinct PKC-mediated posttranscriptional events set cytokine production kinetics in CD8+ T cells. Proc Natl Acad Sci U S A 114, 9677–9682 (2017). [PubMed: 28835535]
16. Hodge DL et al. IFN-gamma AU-rich element removal promotes chronic IFN-gamma expression and autoimmunity in mice. J Autoimmun (2014).
17. Kontoyiannis D, Pasparakis M, Pizarro TT, Cominelli F & Kollias G Impaired on/off regulation of TNF biosynthesis in mice lacking TNF AU-rich elements: implications for joint and gut-associated immunopathologies. Immunity 10, 387–398 (1999). [PubMed: 10204494]
18. Turner M & Hodson D Regulation of lymphocyte development and function by RNA-binding proteins. Curr Opin Immunol 24, 160–165 (2012). [PubMed: 22326859]
19. Kafasla P, Skliris A & Kontoyiannis DL Post-transcriptional coordination of immunological responses by RNA-binding proteins. Nat Immunol 15, 492–502 (2014). [PubMed: 24840980]
20. Salerno F & Wolkers MC T-cells require post-transcriptional regulation for accurate immune responses. Biochemical Society transactions 43, 1201–1207 (2015). [PubMed: 26614661]

21. Bronevetsky Y et al. T cell activation induces proteasomal degradation of Argonaute and rapid remodeling of the microRNA repertoire. The Journal of experimental medicine 210, 417–432 (2013). [PubMed: 23382546]
22. Wu H et al. miRNA profiling of naive, effector and memory CD8 T cells. PloS one 2, e1020 (2007).
23. Garneau NL, Wilusz J & Wilusz CJ The highways and byways of mRNA decay. Nat Rev Mol Cell Biol 8, 113–126 (2007). [PubMed: 17245413]
24. Grammatikakis I, Abdelmohsen K & Gorospe M Posttranslational control of HuR function. Wiley Interdiscip Rev RNA (2016).
25. Jeltsch KM et al. Cleavage of roquin and regnase-1 by the paracaspase MALT1 releases their cooperatively repressed targets to promote T(H)17 differentiation. Nat Immunol 15, 1079–1089 (2014). [PubMed: 25282160]
26. Vlasova-St Louis I & Bohjanen PR Post-transcriptional regulation of cytokine signaling by AU-rich and GU-rich elements. J Interferon Cytokine Res 34, 233–241 (2014). [PubMed: 24697201]
27. Beisang D & Bohjanen PR Perspectives on the ARE as it turns 25 years old. Wiley Interdiscip Rev RNA 3, 719–731 (2012). [PubMed: 22733578]
28. Schoenberg DR & Maquat LE Regulation of cytoplasmic mRNA decay. Nat Rev Genet 13, 246–259 (2012). [PubMed: 22392217]
29. Zehn D, Lee SY & Bevan MJ Complete but curtailed T-cell response to very low-affinity antigen. Nature 458, 211–214 (2009). [PubMed: 19182777]
30. Penix L, Weaver WM, Pang Y, Young HA & Wilson CB Two essential regulatory elements in the human interferon gamma promoter confer activation specific expression in T cells. The Journal of experimental medicine 178, 1483–1496 (1993). [PubMed: 8228802]
31. Hamilton SE, Wolkers MC, Schoenberger SP & Jameson SC The generation of protective memory-like CD8+ T cells during homeostatic proliferation requires CD4+ T cells. Nat Immunol 7, 475–481 (2006). [PubMed: 16604076]
32. Leppek K & Stoecklin G An optimized streptavidin-binding RNA aptamer for purification of ribonucleoprotein complexes identifies novel ARE-binding proteins. Nucleic acids research 42, e13 (2014).
33. Brooks SA & Blackshear PJ Tristetraprolin (TTP): interactions with mRNA and proteins, and current thoughts on mechanisms of action. Biochimica et biophysica acta 1829, 666–679 (2013). [PubMed: 23428348]
34. Galloway A et al. RNA-binding proteins ZFP36L1 and ZFP36L2 promote cell quiescence. Science (New York, N.Y 352, 453–459 (2016).
35. Ogilvie RL et al. Tristetraprolin mediates interferon-gamma mRNA decay. J Biol Chem 284, 11216–11223 (2009). [PubMed: 19258311]
36. Taylor GA et al. A pathogenetic role for TNF alpha in the syndrome of cachexia, arthritis, and autoimmunity resulting from tristetraprolin (TTP) deficiency. Immunity 4, 445–454 (1996). [PubMed: 8630730]
37. Hodson DJ et al. Deletion of the RNA-binding proteins ZFP36L1 and ZFP36L2 leads to perturbed thymic development and T lymphoblastic leukemia. Nat Immunol 11, 717–724 (2010). [PubMed: 20622884]
38. Lindstein T, June CH, Ledbetter JA, Stella G & Thompson CB Regulation of lymphokine messenger RNA stability by a surface-mediated T cell activation pathway. Science (New York, N.Y 244, 339–343 (1989).
39. Ma F et al. The microRNA miR-29 controls innate and adaptive immune responses to intracellular bacterial infection by targeting interferon-gamma. Nat Immunol 12, 861–869 (2011). [PubMed: 21785411]
40. Steiner DF et al. MicroRNA-29 regulates T-box transcription factors and interferon-gamma production in helper T cells. Immunity 35, 169–181 (2011). [PubMed: 21820330]
41. Fleischer TC, Weaver CM, McAfee KJ, Jennings JL & Link AJ Systematic identification and functional screens of uncharacterized proteins associated with eukaryotic ribosomal complexes. Genes Dev 20, 1294–1307 (2006). [PubMed: 16702403]

42. Mackay LK et al. Hobit and Blimp1 instruct a universal transcriptional program of tissue residency in lymphocytes. Science (New York, N.Y 352, 459–463 (2016).
43. Hudson BP, Martinez-Yamout MA, Dyson HJ & Wright PE Recognition of the mRNA AU-rich element by the zinc finger domain of TIS11d. Nat Struct Mol Biol 11, 257–264 (2004). [PubMed: 14981510]
44. Goldrath AW et al. Cytokine requirements for acute and Basal homeostatic proliferation of naive and memory CD8+ T cells. The Journal of experimental medicine 195, 1515–1522 (2002). [PubMed: 12070279]
45. Hochweller K et al. Dendritic cells control T cell tonic signaling required for responsiveness to foreign antigen. Proc Natl Acad Sci U S A 107, 5931–5936 (2010). [PubMed: 20231464]
46. Swamy M et al. A Cholesterol-Based Allostery Model of T Cell Receptor Phosphorylation. Immunity 44, 1091–1101 (2016). [PubMed: 27192576]
47. Abdelsamed HA et al. Human memory CD8 T cell effector potential is epigenetically preserved during in vivo homeostasis. The Journal of experimental medicine 214, 1593–1606 (2017). [PubMed: 28490440]
48. Piecyk M et al. TIA-1 is a translational silencer that selectively regulates the expression of TNF-alpha. EMBO J 19, 4154–4163 (2000). [PubMed: 10921895]
49. Gruber AR, Fallmann J, Kratochvill F, Kovarik P & Hofacker IL AREsite: a database for the comprehensive investigation of AU-rich elements. Nucleic acids research 39, D66–69 (2011). [PubMed: 21071424]
50. Stetson DB et al. Constitutive cytokine mRNAs mark natural killer (NK) and NK T cells poised for rapid effector function. The Journal of experimental medicine 198, 1069–1076 (2003). [PubMed: 14530376]
51. Gessner A, Mohrs K & Mohrs M Mast cells, basophils, and eosinophils acquire constitutive IL-4 and IL-13 transcripts during lineage differentiation that are sufficient for rapid cytokine production. J Immunol 174, 1063–1072 (2005). [PubMed: 15634931]
52. Villarino AV et al. Posttranscriptional silencing of effector cytokine mRNA underlies the anergic phenotype of self-reactive T cells. Immunity 34, 50–60 (2011). [PubMed: 21236706]
53. Hombrink P et al. Programs for the persistence, vigilance and control of human CD8+ lung-resident memory T cells. Nat Immunol (2016).

METHODS-ONLY REFERENCES

54. Zhang L et al. ZFP36L2 is required for self-renewal of early burst-forming unit erythroid progenitors. Nature 499, 92–96 (2013). [PubMed: 23748442]
55. Lee PP et al. A critical role for Dnmt1 and DNA methylation in T cell development, function, and survival. Immunity 15, 763–774 (2001). [PubMed: 11728338]
56. Brummelkamp TR, Bernards R & Agami R Stable suppression of tumorigenicity by virus-mediated RNA interference. Cancer Cell 2, 243–247 (2002). [PubMed: 12242156]
57. Kessels HW, Wolkers MC, van den Boom MD, van der Valk MA & Schumacher TN Immunotherapy through TCR gene transfer. Nat Immunol 2, 957–961 (2001). [PubMed: 11577349]
58. Salerno F, Guislain A, Cansever D & Wolkers MC TLR-Mediated Innate Production of IFN-gamma by CD8+ T Cells Is Independent of Glycolysis. J Immunol 196, 3695–3705 (2016). [PubMed: 27016606]
59. McCausland MM et al. SAP regulation of follicular helper CD4 T cell development and humoral immunity is independent of SLAM and Fyn kinase. J Immunol 178, 817–828 (2007). [PubMed: 17202343]
60. Lopez de Silanes I, Zhan M, Lal A, Yang X & Gorospe M Identification of a target RNA motif for RNA-binding protein HuR. Proc Natl Acad Sci U S A 101, 2987–2992 (2004). [PubMed: 14981256]
61. Rappsilber J, Ishihama Y & Mann M Stop and go extraction tips for matrix-assisted laser desorption/ionization, nanoelectrospray, and LC/MS sample pretreatment in proteomics. Anal Chem 75, 663–670 (2003). [PubMed: 12585499]

62. Kulak NA, Pichler G, Paron I, Nagaraj N & Mann M Minimal, encapsulated proteomic-sample processing applied to copy-number estimation in eukaryotic cells. Nat Methods 11, 319–324 (2014). [PubMed: 24487582]

63. Cox J & Mann M MaxQuant enables high peptide identification rates, individualized p.p.b.-range mass accuracies and proteome-wide protein quantification. Nat Biotechnol 26, 1367–1372 (2008). [PubMed: 19029910]

64. Love MI, Huber W & Anders S Moderated estimation of fold change and dispersion for RNA-seq data with DESeq2. Genome Biol 15, 550 (2014). [PubMed: 25516281]

65. Di Tommaso P et al. T-Coffee: a web server for the multiple sequence alignment of protein and RNA sequences using structural information and homology extension. Nucleic acids research 39, W13–17 (2011). [PubMed: 21558174]

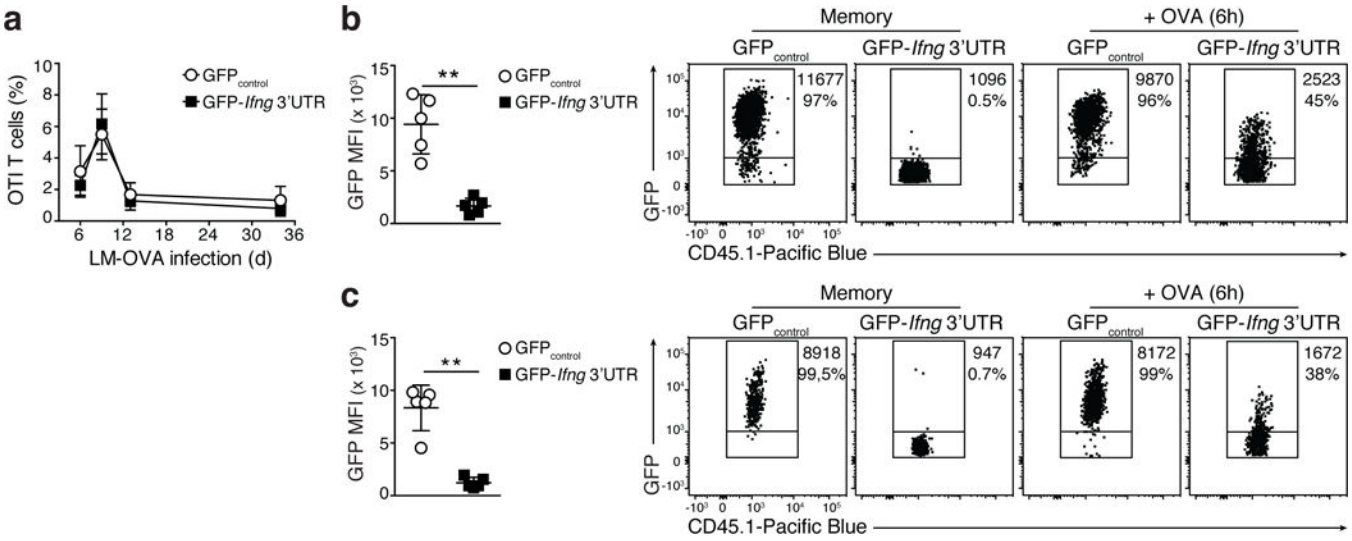

Figure 1: The 3'UTR of *Ifng* governs GFP expression in memory T cells *in vivo*

(**a**) Blood samples of LM-OVA infected C57BL/6J/CD45.2 recipient mice were analyzed for the presence of CD45.1$^+$ OTI cells expressing GFP-*Ifng* 3'UTR or $GFP_{control}$ reporter (n=10/group). GFP-MFI levels measured directly *ex vivo* in (**b**) spleen- and in (**c**) liver-residing OTI cells 35 days after infection. [Unpaired Student *t*-test; n=5 mice per group; **p<0.005]. Representative GFP expression in memory OTI cells directly *ex vivo* (memory), and upon reactivation with $OVA_{257–264}$ peptide (+ OVA (6h)). Numbers in plots depict the GFP-MFI of the total population (top number) and the percentage of T cells within the upper gate that express high GFP levels (bottom number). Data shown are representative of 2 independently performed experiments.

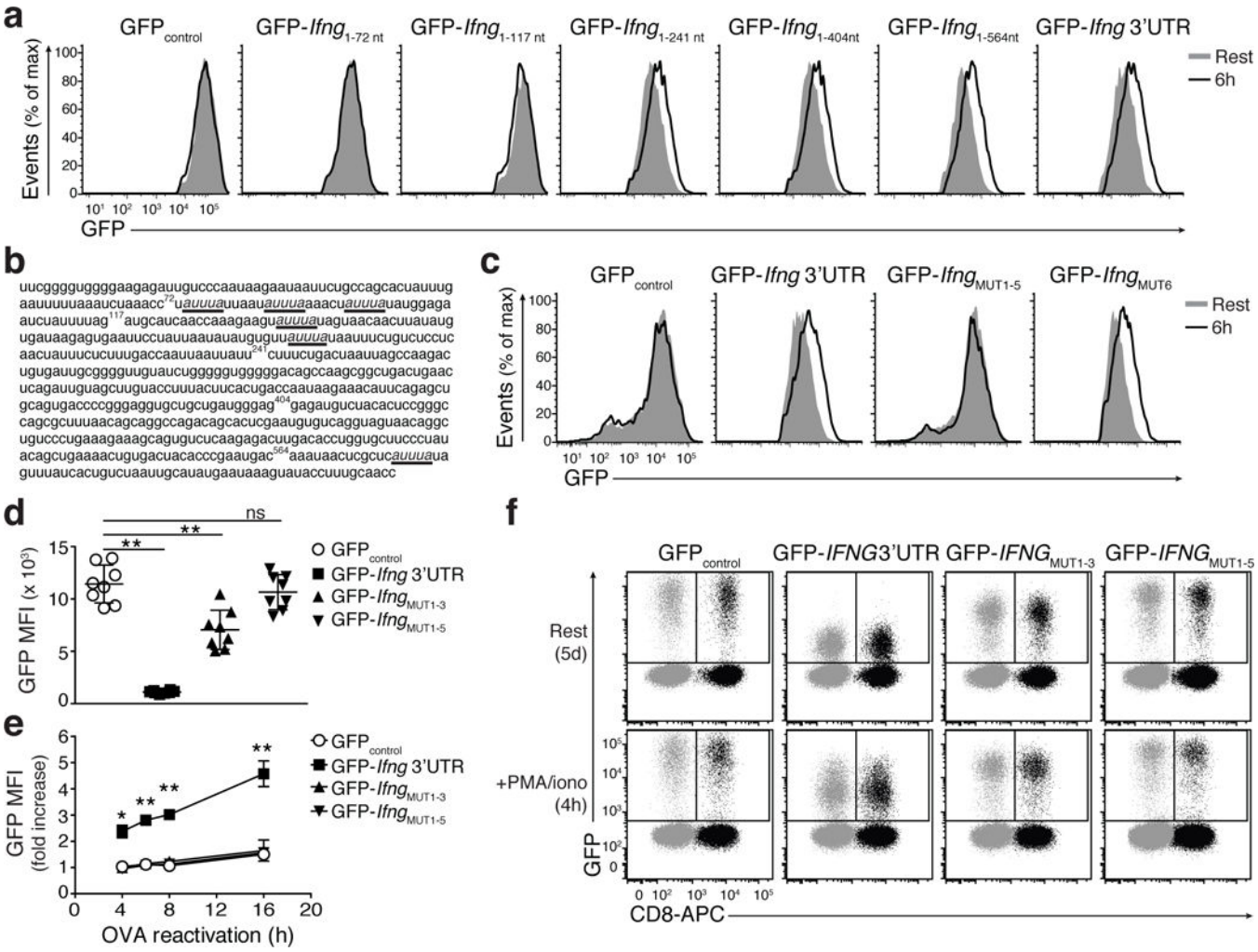

Figure 2: AU-rich elements within the *Ifng* 3'UTR determine protein production in mouse and human T cells

OTI cells were transduced with deletion mutants (**a**) or with ARE mutants of the full length murine *Ifng* 3'UTR (**c-e**). (**b**) Sequence of the murine *Ifng* 3'UTR. AREs are underlined. (**a,c**) Representative GFP levels of resting OTI cells (gray histograms), and after reactivation with $OVA_{257–264}$ peptide for 6h (black lines). (**d**) GFP-MFI of resting OTI cells transduced with indicated ARE mutants. (**e**) Fold increase of GFP-MFI upon activation with $OVA_{257–264}$ peptide compared to non-activated GFP-expressing T cells. (**d-e**) Data are presented as mean±SD of at least 3 independently performed experiments [one-way ANOVA with Dunnett's multiple comparison to the control vector; n=8 mice per group; *p<0.005; **p<0.0005]. (**f**) Human T cells were transduced with full length human GFP-*IFNG* 3'UTR (WT), or with ARE mutants. Dot plots depicting GFP-MFI levels from resting T cells (top), or from PMA/ionomycin reactivated T cells (bottom), with $CD8^+$ T cells shown in black and $CD4^+$ T cells in gray. Data shown are representative of 4 individuals, and of 3 independently performed experiments. Compiled data are depicted in Supplementary Fig. 2d.

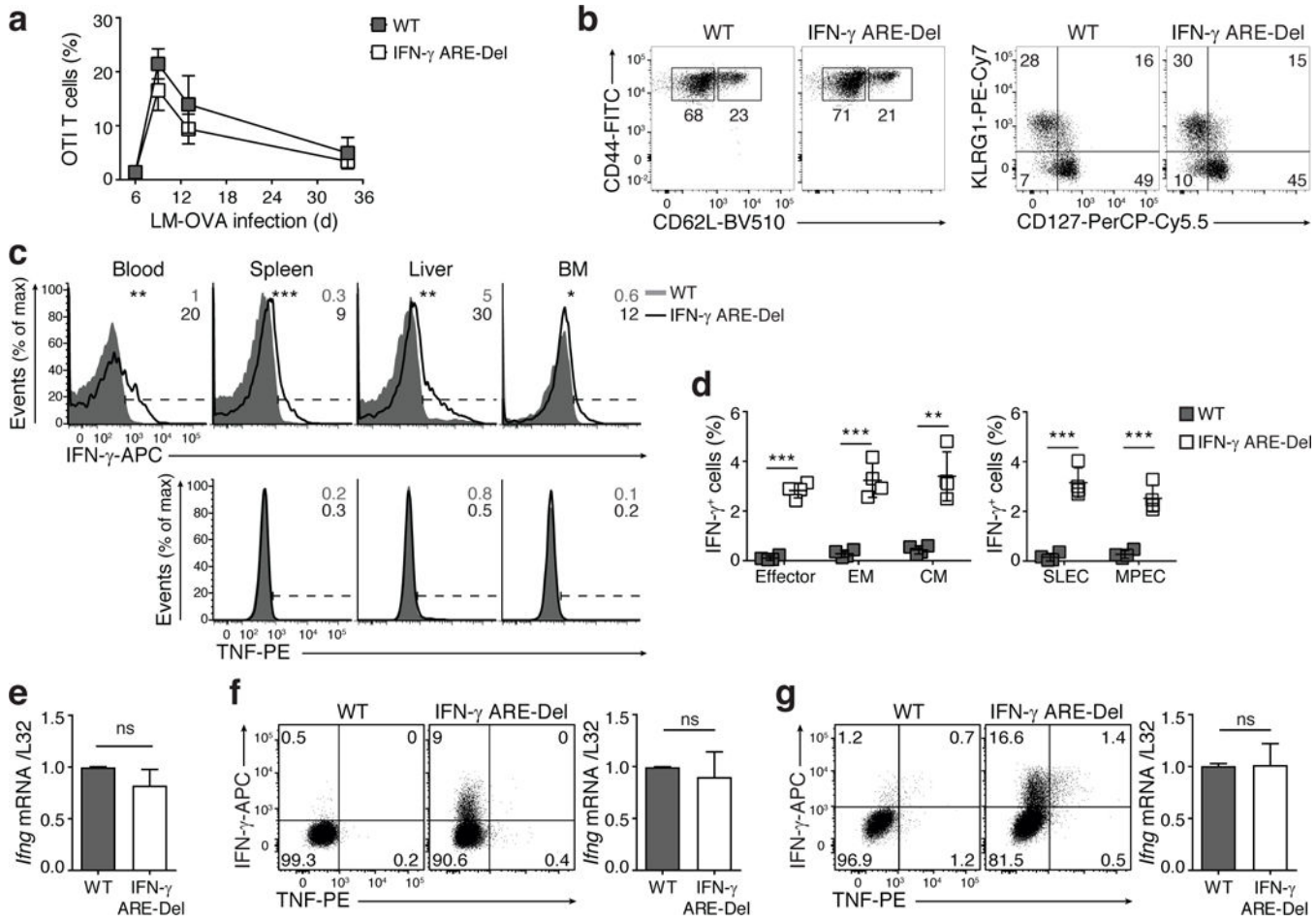

Figure 3: Deletion of AREs in the *Ifng* 3'UTR dysregulates protein production in T_M cells

(**a**) Percentage of $CD8^+$OTI cells in blood drawn from LM-OVA infected mice at indicated time points (n=8 mice/group). (**b**) Representative dot plots of CD44/CD62L expression (left) and of CD127/KLRG1 expression (right) of wild-type OT-I/CD45.1 and IFN-γ-ARE-Del OT-I/CD45.2 cells 35 days post LM-OVA infection. Numbers in dot plots indicate percentage of OTI cells in corresponding gates. Compiled data are depicted in Supplementary Fig. 3a. (**c**) IFN-γ and TNF production measured in blood, spleen, liver, and bone marrow (BM)-derived T_M cells after 3h incubation with 1μg/ml BFA. Histograms represent wild-type OT-I/CD45.1 (gray histograms) and IFN-γ-ARE-Del OT-I/CD45.2 (black lines) T_M cells. Numbers depict percentage of IFN-γ^+ and TNF-producing$^+$ T cells. IFN-γ and TNF MFI of wild-type and IFN-γ-ARE-Del T cells was compared with an Unpaired Student *t*-test [n=4 mice/group; *p<0.05; **p<0.005; ***p<0.0005]. (**d**) Percentage of IFN-γ producing T cells from spleen-residing wild-type (gray square) and IFN-γ-ARE-Del (white square) $CD44^{hi}CD62L^{lo}CD\ 127^{lo}$ T_{EFF}, $CD44^{hi}CD62L^{lo}CD127^{hi}$ T_{EM}, $CD44^{hi}CD62L^{hi}CD127^{hi}$ T_{CM}, $KLRG1^{hi}CD127^{lo}$ SLEC and $KLRG1^{lo}CD127^{hi}$ MPEC cells 35 days post LM-OVA infection. [Unpaired Student *t*-test; n=4 mice/group; **p<0.005; ***p<0.0005]. (**e**) *Ifng* mRNA expression in sorted splenic wild-type or IFN-γ-ARE-Del OT-I T_M cells 35 days post LM-OVA infection (pooled from 4 mice). Pooled data from 2 independently performed experiments. (**f-g**) IFN-γ protein (left) and mRNA levels

(right) of sorted spleen (**f**) and liver (**g**)-derived $CD44^{hi}CD8^{+}$ wild-type and IFN-γ-ARE-Del OT-I cells. Representative dot plots of 4 mice. mRNA data are pooled from 4 independently performed experiments. (**e**-**g**) [Unpaired Student *t*-test; ns=not significant].

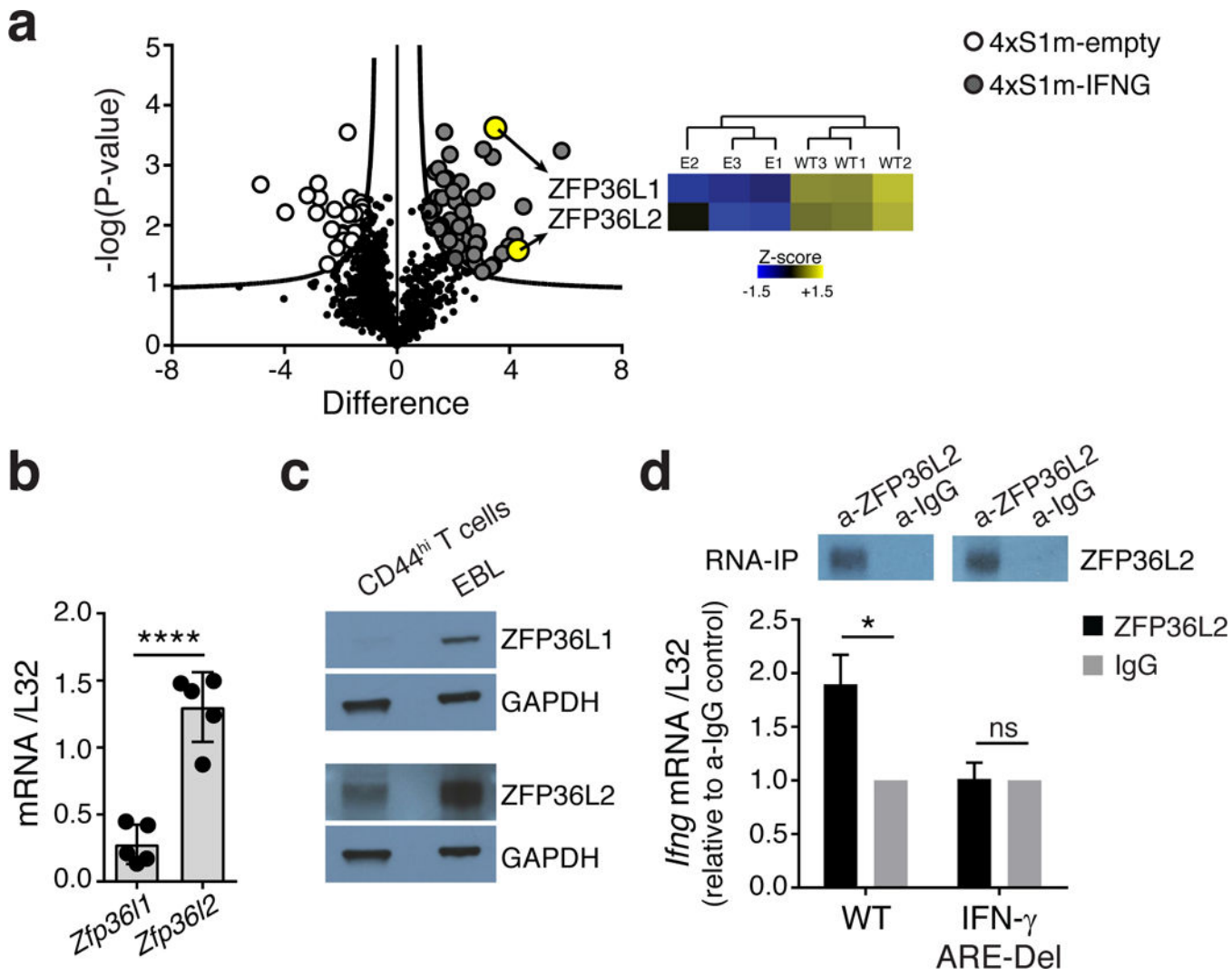

Figure 4: The RNA-binding protein ZFP36L2 binds *Ifng* mRNA

(**a**) Volcano plot of RBPs quantified by mass spectrometry from human resting T cell lysates pulled down with *in vitro* transcribed 4xS1m mRNA containing the 189nt long ARE-region of the human *IFNG* 3'UTR (4xS1m-*IFNG*), and the empty 4xS1m mRNA control (4xS1m-empty). Only proteins identified in all three replicates were considered putative ARE binders. Gray dots represent proteins that were significantly enriched in the presence of the *IFNG* 3'UTR, white dots represent proteins enriched in 4xS1m-empty [Two-sided *t*-test; FDR=0.05, S0=0.4)]. Heat map depicts Z-scored log2 LFQ values of ZFP36L1 and ZFP36L2 in all three replicates. (**b-c**) mRNA (**b**) and protein (**c**) expression of ZFP36L1 and ZFP36L2 in CD44^{hi}CD8^{+} T cells. For the Western Blot, erythroblasts (EBL) were used as positive control[54]. (**d**) Binding of ZFP36L2 to *Ifng* mRNA in resting wild-type and IFN-γ-ARE-Del OTI cells was analyzed by RNA-immunoprecipitation. IgG isotype was used as control. Top: ZFP36L2 protein expression upon RNA-IP, detected with a pan anti-ZFP36 antibody at ±55KD (specific size of ZFP36L2). Bottom: Data are pooled from 3 independently performed experiments (mean±SD) [Unpaired Student *t*-test; n=4 mice/group; ns=not significant; *p<0.05].

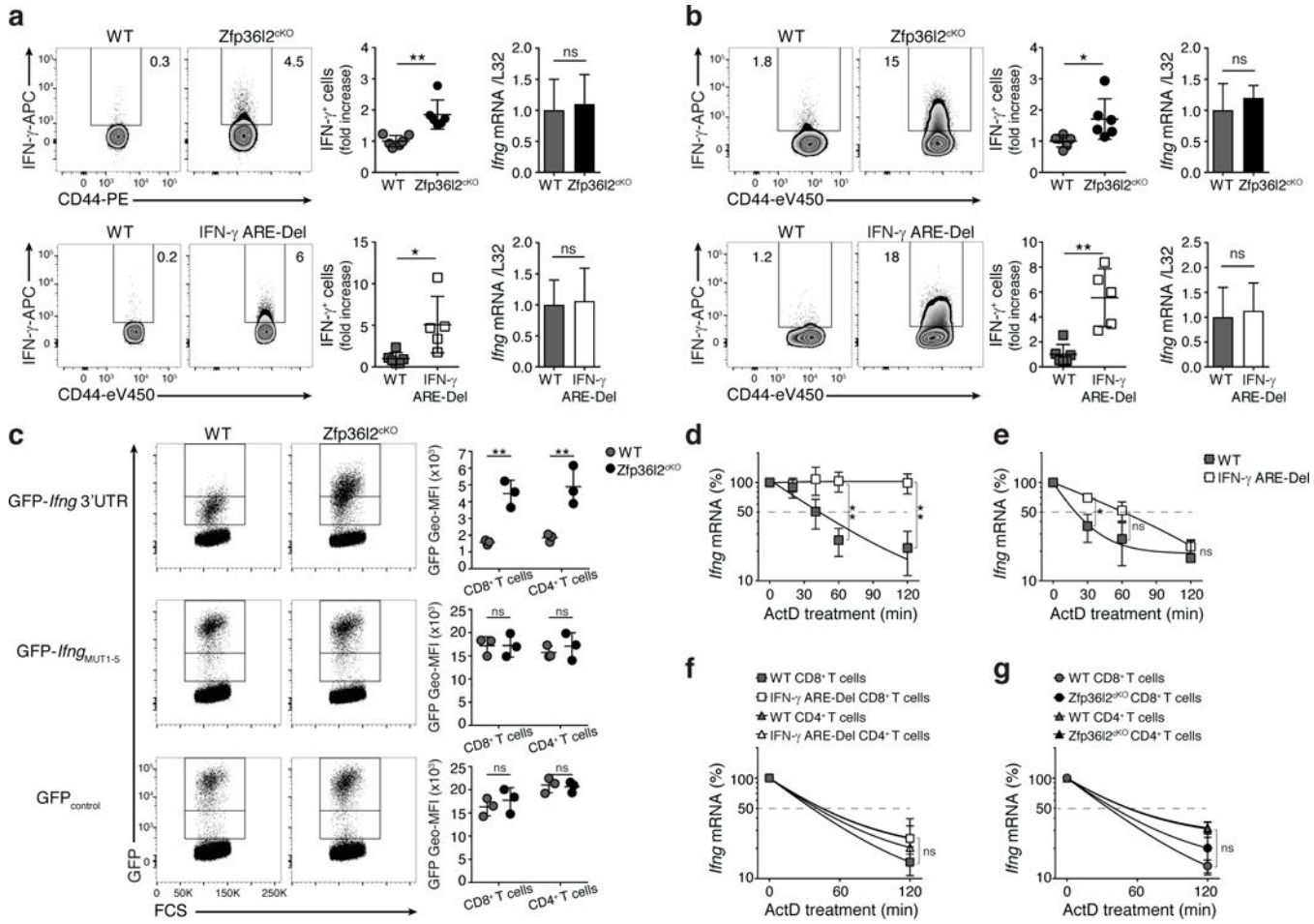

Figure 5: The ARE-binding protein ZFP36L2 represses IFN-γ production in T_M cells

(**a-b**) IFN-γ production of sorted splenic $CD44^{hi}CD8^+$ (**a**), and $CD44^{hi}CD4^+$ (**b**) T cells from $Zfp36l2^{cKO}$ mice compared to wild-type littermates after 3h of incubation with BFA (upper panel; n=6 mice/group), and IFN-γ-ARE-Del mice compared to C57BL/6J wild-type mice (lower panel; n=5 mice/group). Left: representative dot plot. Middle: compiled data (mean±SD) depicting the fold increase of IFN-γ production compared to wild-type mice. Right: *Ifng* mRNA expression levels±SD. (**c**) T cells from $Zfp36l2^{cKO}$ mice and wild-type littermates were retrovirally transduced with GFP-*Ifng* 3'UTR, $GFP_{MUT1–5}$, or $GFP_{control}$. Left: dot plots represent GFP expression of $CD8^+$ T cells. Right: GFP Geo-MFI of $CD8^+$ and $CD4^+$ T cells that were rested in rmIL-7 for 5 days (n=3 mice/group; mean±SD). (**d-e**) *Ifng* mRNA levels of *in vitro* resting OTI cells (**d**) or *ex vivo* sorted $CD44^{hi}CD8^+$ OTI cells (**e**) after treatment with 1μg/ml ActD for the indicated time points. Results±SD are pooled from 4 independently performed experiments (n=4 mice/group). (**f-g**) *Ifng* mRNA stability was assessed upon ActD treatment of $CD44^{hi}CD8^+$ T cells or $CD44^{hi}CD4^+$ T cells from IFN-γ-ARE-Del (**f**; n=5 mice/group) or $Zfp36l2^{cKO}$ (**g**; n=3 mice/group) mice and their respective wild-type controls. Results±SD are pooled from 2 independently performed experiments. For individual data points see Supplementary Fig. 5f,g. (**a-h**) [Unpaired Student *t*-test; ns=not significant; *p<0.05; **p<0.005].

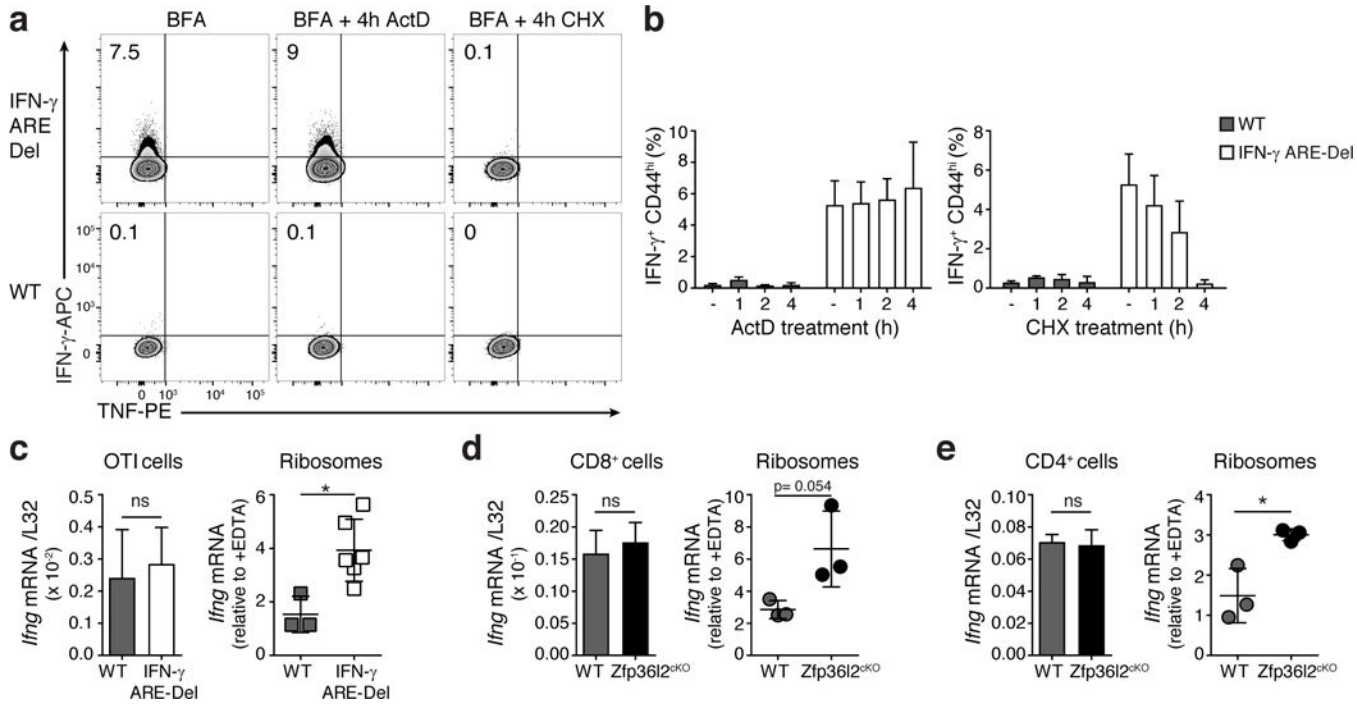

Figure 6: The interaction between AREs and ZFP36L2 blocks ribosome recruitment of pre-formed *Ifng* mRNA

(**a**) Representative IFN-γ and TNF production of sorted CD44^{hi}CD8^{+} memory-like IFN-γ-ARE-Del (upper panel) and wild-type (lower panel) OTI cells after 4h incubation with BFA alone (left), or with 1μg/ml ActD (middle) or 10μg/ml CHX (right). (**b**) Graphs depict percentage (mean±SD of 4 independently performed experiments) of IFN-γ producing CD44^{hi}CD8^{+} wild-type or IFN-γ-ARE-Del OTI cells incubated with or without ActD (left) or CHX (right) for the entire culture of 4h, or for the last 2 or 1h. (**c-e**) *Ifng* mRNA levels of cytosolic fractions from (**c**) CD44^{hi}CD8^{+} wild-type or IFN-γ-ARE-Del OTI cells, (**d**) CD44^{hi}CD8^{+} T cells or (**e**) CD44^{hi}CD4^{+} T cells from Zfp36l2^{cKO} or wild-type littermates. Left: mRNA input prior to fractionation; right: mRNA measured in the ribosome-enriched fraction after centrifugation of a sucrose cushion. Ribosome binding was determined by correlating the mRNA levels from untreated cytosolic fractions with that of EDTA-treated fractions. Results (mean±SD) are pooled from 3 (**c**; n=3–6 mice) and 2 (**d-e**; n=3 mice) independently performed experiments. [Unpaired Student *t*-test; ns=not significant; *p<0.05].

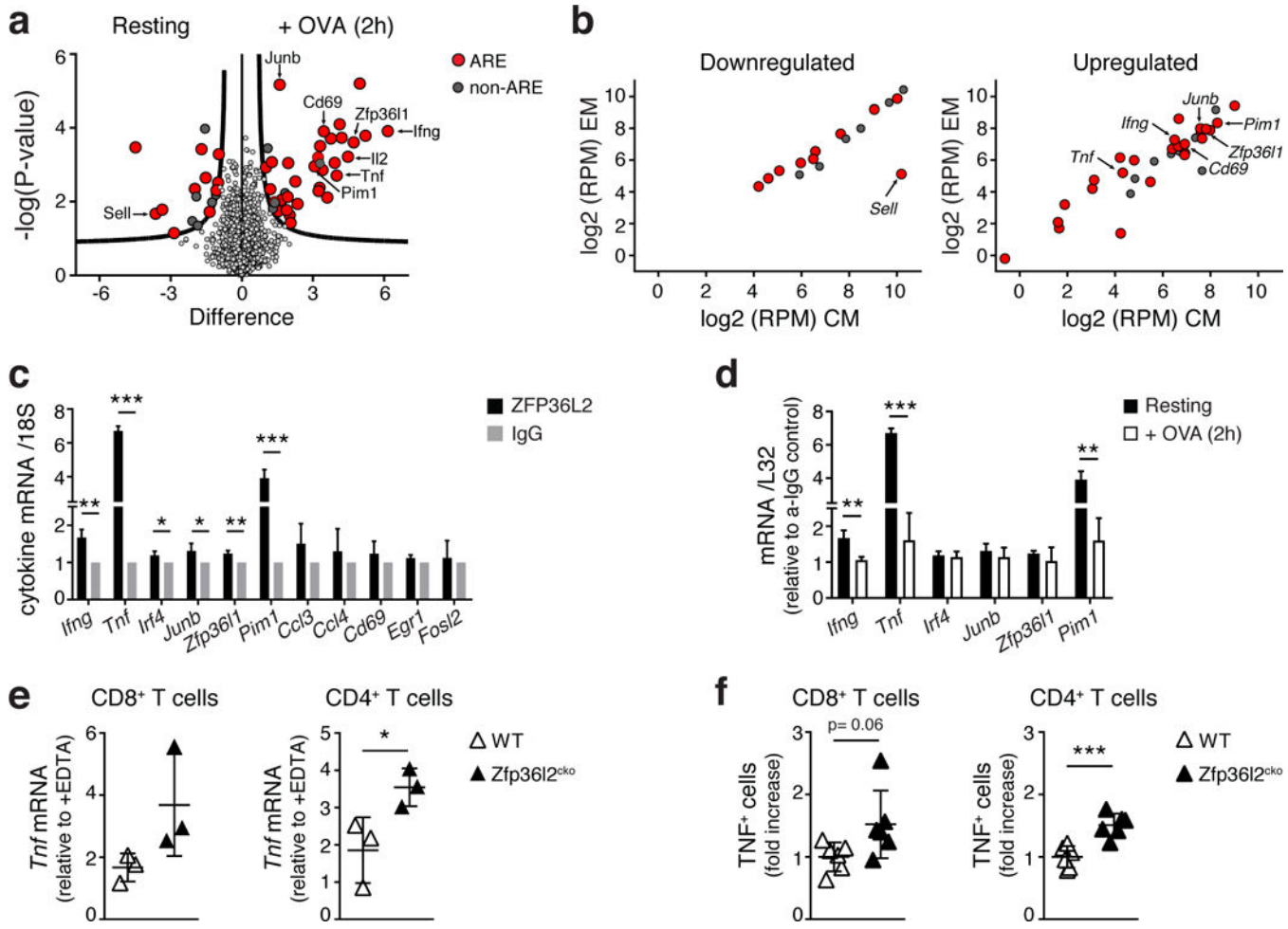

Figure 7: ZFP36L2 blocks translation of pre-formed mRNA from rapidly generated effector molecules

(**a**) Volcano plot of proteins quantified by mass spectrometry from splenic CD44^{hi}CD8^{+} OTI cells that were cultured for 2h with or without 100nM of OVA$_{257–264}$ peptide in the presence of 1μg/ml BFA [n=3; Two-sided *t*-test; FDR=0.05, S0=0.4)]. (**b**) mRNA expression of LCMV-specific spleen-derived T_{EM} and T_{CM} cells from ref.[53]. Graphs display log2-normalized counts of reads per million mapped reads (RPM), of which in panel **a** protein expression was significantly downregulated (left), or upregulated (right) upon T cell activation. (**a-b**) Red dots depict proteins that are encoded by ARE-containing transcripts. (**c-d**) ZFP36L2 RNA-immunoprecipitation of resting OTI cells compared to anti-IgG control RNA-IP (**c**) or compared to RNA-IP from cells reactivated for 2h with 100nM of OVA$_{257–264}$ peptide (values from anti-IgG control RNA-IP was substracted from each value) (**d**). Data are presented as mean±SD of 3–4 mice and pooled from 3 independently performed experiments. (**e-f**) CD44^{hi}CD8^{+} and CD4^{+} T cells were sorted from Zfp36l2^{cKO} or wild-type littermates. (**e**) Ribosome-bound *Tnf* mRNA was measured by RT-PCR following centrifugation through a sucrose cushion. Graphs display mRNA expression levels relative to paired EDTA-treated control samples (n=3). (**f**) Spontaneous TNF protein production was depicted as fold increase compared to wild-type mice (n=6). Results are

pooled from 2 independently performed experiments. (**c-f**) [Unpaired Student *t*-test; *p<0.05; ***p<0.0005].